Journal of Alloys and Compounds 900 (2022) 163533

Contents lists available at ScienceDirect

Journal of Alloys and Compounds

journal homepage: www.elsevier.com/locate/jalcom

Research Article

# Computing the iron–nitrogen phase diagram at high pressure and high temperature

Hanof Alkhaldi, Peter Kroll*

*Department of Chemistry and Biochemistry, The University of Texas at Arlington, 700 Planetarium Place, Arlington, TX 76019, United States*

ARTICLE INFO

*Article history:*
Received 13 September 2021
Received in revised form 27 December 2021
Accepted 28 December 2021
Available online 30 December 2021

*Keywords:*
High-pressure iron-nitrogen compounds
Phase diagram
Chemical potential nitrogen

ABSTRACT

Locating pressure and temperature conditions relevant to concurrent diamond-anvil-cell (DAC) experiments is imperative for the discovery of new high–pressure nitrogen-rich compounds. In this work we provide a pressure-temperature phase diagram of the iron–nitrogen system for pressures up to 200 GPa and temperatures up to 4000 K through a combination of Density Functional Theory computations and thermodynamic calculations. The work includes an assessment of the chemical potential of nitrogen and its change at high pressure and high temperature. We deliver stability fields of various Fe–N compounds in the presence of excess nitrogen. Our results are in agreement with recent synthesis of $FeN_2$ and $FeN_4$, and predict a hitherto unknown $FeN_8$ attainable at 100 GPa and 1500 K.



## 1. Introduction

A variety of new nitrogen-rich compounds of main group elements and transition metals have been synthesized over the last two decades [1–12]. Advances in experimental techniques to attain high pressure/high temperature (HPHT) conditions facilitate this progress, in good parts driven and supported by computational studies [1,13–15]. New transition metal nitrogen (TM-N) compounds include nitrides [3], pernitrides [16], mixed nitride-pernitrides, compounds comprising complex polyatomic nitrogen anions, and compounds with extended anionic nitrogen chains [7].

The iron-nitrogen system is particularly relevant to industrial applications [17] as well as to planetary cores [18–22]. Binary Fe–N compounds synthesized at ambient pressure include crystalline structures of $Fe_4N$, $Fe_3N$, and $Fe_2N$ [23–25]. Recently, more nitrogen–rich compounds $Fe_3N_2$, FeN, $FeN_2$, and $FeN_4$ have been synthesized at high pressure and high temperature [7,26–30]. Much computational work has been devoted to investigate these and to identify further Fe-N polymorphs. This includes structures of $Fe_4N$, $Fe_3N$, $Fe_4N_3$, $Fe_7N_3$, $Fe_2N$, FeN, $FeN_2$, $FeN_4$, $FeN_6$ $FeN_8$, and $FeN_{10}$ [31–36]. Computed data has been used to construct composition–formation enthalpy convex hulls of the Fe–N system for pressures up to 300 GPa, and based on those several phase transitions of nitrogen–rich Fe-N compounds have been proposed [32,33,37]. For instance, the most favorable structure of FeN at ambient pressure is a ZnS-type structure (sp.gr. *F*4–3*m* (216)), which transfers to a NiAs-type structure (sp.gr. $P6_3/mmc$ (194)) at about 24 GPa. The NiAs-type of FeN exhibits remarkable magnetic properties even at high pressure [38]. At 79 GPa a MnP-type structure of FeN (sp.gr. *Pnma* (62)) then becomes preferred. A marcasite-type structure of $FeN_2$ (sp.gr. *Pnmm* (194)) was proposed to become accessible above 22 GPa, and a $FeN_4$ (sp.gr. *P*-1 (2)) with unprecedented structure above 30 GPa [32,33,37]. Notably, both compounds $FeN_2$ and $FeN_4$ were subsequently synthesized in high pressure experiments [7,28,29]. Other Fe-N polymorphs proposed to be attainable up to 300 GPa include $Fe_3N_8$, $FeN_3$, $FeN_6$, and $FeN_8$ [32,33,37].

The target of our contribution is to explore thermodynamic stability of Fe–N compounds at experimental conditions and, thus, to provide a useful guide for experimentalists. In a typical high pressure synthesis experiment iron is placed into a diamond anvil cell, which is then loaded with nitrogen [7,39]. Excess nitrogen in the cell acts both as pressure transmitting medium as well as reactant. After compression to a desired pressure, the iron is heated by irradiation through a laser-heating system to overcome activation barriers and enable reactions with nitrogen at high pressures. To achieve our goal, we combine quantum-chemical and thermodynamic calculations to provide a pressure–temperature phase diagram of Fe–N under excess nitrogen. The phase diagram predicts synthesis conditions of thermodynamically stable Fe–N phases accessible through DAC experiments using nitrogen as pressure medium.

* Corresponding author.
*E-mail address:* pkroll@uta.edu (P. Kroll).

https://doi.org/10.1016/j.jallcom.2021.163533
0925-8388/

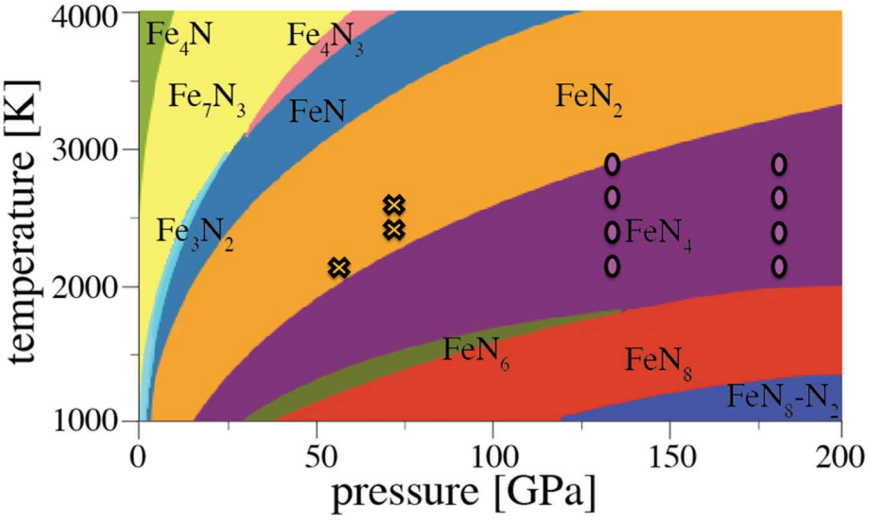


**Fig. 1.** The iron-nitrogen pressure-temperature phase diagram computed by combining of first principles (SCAN functional) and thermodynamic calculations. Experimental conditions reported for the formation of $FeN_2$ [7,28] and of $FeN_4$ [7,29] are indicated by crosses and circles, respectively.

## 2. Computational method

All calculations of total energy are performed within Density Functional Theory (DFT) as implemented in Vienna Ab-initio Simulation Package (VASP) [40–43]. We use pseudopotentials based on the projector-augmented-wave (PAW) method [44,45]. We apply strongly constrained and appropriately normed semilocal density functional (SCAN) [46]. With the goal to predict phase boundaries at temperatures well above 1000 K, we do not explicitly search for magnetic order. Hence, calculations are performed without spin-polarization. The Brillouin zone of each structure is sampled by k-point meshes with grid sizes smaller than 0.03 $Å^{-1}$. All calculations depend on well forces converged to better than 1 meV/Å with a plane wave cut-off energy of (500 eV) which yields energy and enthalpy differences between structures converged to better than 1 meV per atom.

We started our endeavor by computing Fe–N structures reported previously [7,26,28,29,37,47]. We then used the Universal Structure Predictor Evolutionary Xtallography (USPEX) [48] code to identify known and to locate potential new polymorphs. For the structure searches by USPEX we start with variable composition searches at 80 GPa to identify potential compositions with high nitrogen content. Ensembles of 50 structures are followed for 20 generations. For each new generation, 40% of structures are taken by heredity, 20% randomly, 20% through lattice mutations, and 20% by atom mutation. This process is repeated with new seed structures 20 times. Promising compositions – identified by negative enthalpy of formation (from elements and/or from neighboring compositions) at least at some pressure – are followed in more detail with searches at constant composition. This includes compositions with high nitrogen content such as $FeN_4$, $FeN_6$ and $FeN_8$. We search crystal structures with at least 20 atoms in their primitive unit cell and perform (at least each 20 independent) searches at 40, 80, 120, and 160 GPa. Ensembles of 15–25 structures are evolved for up to 45 generations (50% heredity, 10% random, 20% lattice mutations, 20 at. mutations). We augmented the structure data base by models obtained earlier for different transition metal nitride compounds [49]. The most nitrogen–rich composition we studied was $FeN_{10}$. It turns out that all structures encountered in this study have been reported before, with exception of a new polymorph of $FeN_8$.

Enthalpy-pressure data of every structure is acquired using standard techniques described earlier [50]. In brief: energy–volume data of each structure is converted to enthalpy-pressure data by numerical differentiation. For all reaction involving solid state structures the enthalpy of reaction $\Delta H$ is equated to reaction Gibbs energies $\Delta G$, because entropy changes that contribute to $\Delta G$ are much smaller than changes of $\Delta H$ within a few GPa of pressure. For reaction involving nitrogen, we augment reaction Gibbs energies $\Delta G$ with chemical potential changes of nitrogen, $\Delta\mu(p,T)$, as outlined in previous studies [51,52]. Experimental data of $\Delta\mu(p,T)$ for nitrogen is available for low pressures from the freezing point to 4000 K [53]. The data is extrapolated to high pressure and high temperature using the “moderate extrapolation” for fugacity of nitrogen [51]. As result we obtain quantitative data of chemical potential for every phase system and can compare reaction Gibbs energies at high pressure and high temperature conditions. Note that the approach assumes the presence of an excess of nitrogen as reactant, hence it applies to a standard experiment in a diamond-anvil-cell (DAC) loaded with nitrogen. The approach has shown good agreement between experiment and calculations for several systems to at least 80 GPa [52,54]. For instance, it provides a rational for the simultaneous appearance of $Ti_3N_4$ and $TiN_2$ within a temperature range between 1800 and 2400 K at 74 GPa [52,55,56].

## 3. Results and discussion

The computed pressure–temperature ($p,T$) phase diagram for the Iron–Nitrogen system is shown in Fig. 1. It is a result of combining first-principles computations of crystal structures with thermodynamic calculations addressing the chemical potential of nitrogen. We emphasize that the phase diagram as shown applies to an experiment carried out under the condition of excess nitrogen.

At low pressure the computed Fe-N phase diagrams displays perovskite-type γ'-$Fe_4N$, which is commonly observed at ambient conditions [23]. Increasing pressure yields $Fe_7N_3$, with a stability field ranging up to 25 and 50 GPa at 3000 and 4000 K, respectively. At such high temperatures magnetism is not expected to play a role, and, consequently, we obtain the orthorhombic structure (sp.gr. *Amm*2 (38)) being preferred over ε-$Fe_7N_3$ in non-magnetic calculations. The thermodynamical stability of $Fe_7N_3$ then prevents appearance of orthorhombic ζ-$Fe_2N$. This $Fe_2N$ phase was synthesized at 10 GPa at 1800 K using diamond anvil cell and laser heating [30]. The next phase we find to become thermodynamically stable in the presence of excess nitrogen, albeit with a very small stability range, is $Fe_3N_2$-II (sp.gr. *Fdd*2 (43) [57]). This polymorph of $Fe_3N_2$ has not been observed in experiments. However, $Fe_3N_2$-I (sp.gr. *Pnma* (62))

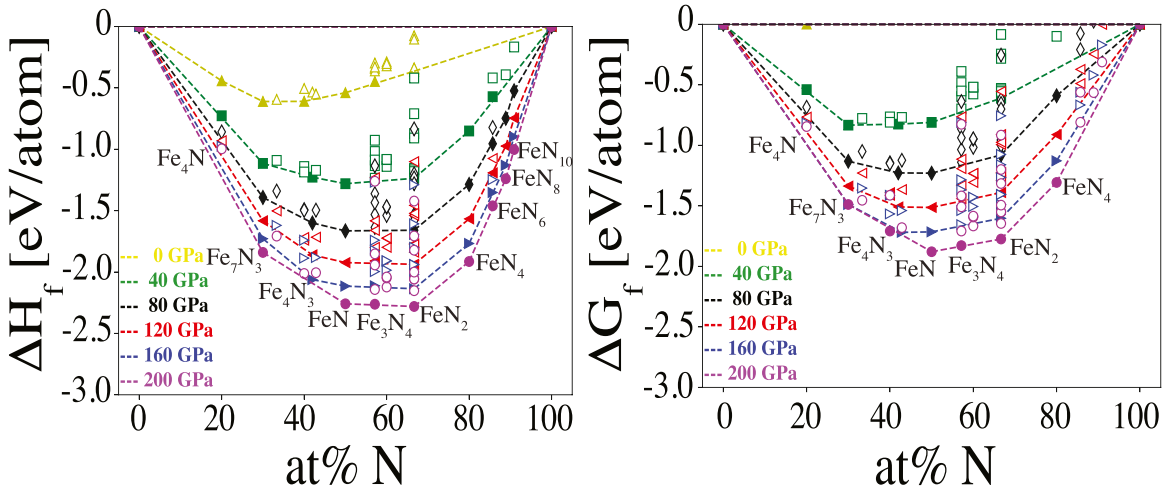


**Fig. 2.** Convex hulls for the Fe-N system at 0, 40, 80, 120,160 and 200 GPa. The diagram on the left refers to formation enthalpy (ΔH, in eV/atom). On the right the diagram refers to formation Gibbs energy (ΔG, in eV/atom) at 2500 K. Phases stable against decomposition into any of its neighboring phases are indicated by filled symbol.

was synthesized at 50 GPa and 1990 K [7]. We find that $Fe_3N_2$-I is a high-pressure phase of $Fe_3N_2$ and will follow $Fe_3N_2$-II as the most favorable $Fe_3N_2$ structure at 80 GPa. In our computed phase diagram $Fe_3N_2$-I does not appear, since at high pressures it is surpassed by phases with higher nitrogen content, FeN, $FeN_2$, and $FeN_4$. We note that at temperatures above 3000 K and pressures between 30 and 70 GPa $Fe_4N_3$ (sp.gr. *Imm*2 (44)) emerges [35]. The well-known FeN (sp.gr. *P*63/*mmc* (194); NiAs-type) follows next. This structure has emerged in various experiments at conditions ranging from 10 to 130 GPa and temperatures from 1300 to 2000 K [7,26,27,39]. We compute its stability range to be smaller, for instance between 10 and 20 GPa at 2000 K. A large part of the phase diagram then is occupied by $FeN_2$ (sp.gr. *Pnmm* (194)) with marcasite-type structure. At 2000 K we compute it to be the thermodynamically most favorable Fe–N compound between 20 and 60 GPa. In experiments this phase was attained at 58.5 GPa and 2100 K [7], but also at 72.5 GPa. Both these experimental conditions are located within the computed stability field for $FeN_2$. At 2000 K and above 60 GPa the only other structure appearing is $FeN_4$ (sp.gr. *P*-1 (2)). This phase has been synthesized at more extreme conditions in experiments, 135 GPa and 2000 K [7,29], and 180 GPa and 2700 K [7]. We have indicated data of reported experimental conditions for the syntheses of $FeN_2$ and $FeN_4$ in Fig. 1. At temperatures below 2000 K and high pressures we find several Fe–N compounds with high nitrogen content displaying infinite nitrogen chains. A small stability range is indicated for monoclinic $FeN_6$ (sp.gr. *C* 2/*m* (12)), a structure predicted earlier [37,58]. At higher pressures $FeN_8$ (sp.gr. (*P*-1 (2) [59])) emerges. This new structure bears similar features – an infinite N-chain and Fe-$N_6$–octahedrons – as the previously suggested modification of $FeN_8$ [37]. However, the coordination environment of Fe is more regular, causing this structure to be lower in enthalpy for all pressures we computed. Finally, we include $FeN_{10}$ (sp.gr. *Immm* (71) [60]), a structure that was first predicted for $HfN_8$-$N_2$ and then synthesized for $ReN_8$-$N_{10}$ and $WN_8$-$N_2$ [49,61].

Previous computational studies in the Fe-N system delivered thermochemical data that was conveniently displayed using the concept of a convex hull [32,33,37]. Note that a typical convex hull in high-pressure science data is based on composition-formation enthalpy data obtained at zero K. Consequently, whenever such diagrams are used to infer "thermodynamic stability" of compounds, the impact of temperature or excess nitrogen is not included in considerations. Using the approach outlined above it is straight forward to attain convex hulls based on Gibbs energy, explicitly including temperature and presence of nitrogen. In Fig. 2 we compare both types of convex hulls, one based on enthalpy and the other based on Gibbs energy at 2500 K. Evidently, the most significant difference between the two diagrams is that several nitrogen-rich Fe-N phases – in particular $FeN_6$, $FeN_8$, and $FeN_{10}$ – are not thermodynamically stable at high pressure at 2500 K. In general, temperature shifts the appearance of a phase on the convex hull (indicating thermodynamic stability) towards higher pressure. This can be seen for $FeN_4$, which appears at 40 GPa on the enthalpy-based convex hull, while it requires more than 80 GPa to appear in the corresponding diagram based on Gibbs energy at 2500 K. A convex hull based on Gibbs energy, therefore, has more predictive power in identifying thermodynamically stable nitrogen-rich phases at the given conditions in the presence of excess nitrogen.

Phase diagrams as that shown in Fig. 1 display phases with minimum Gibbs energy at a given *p,T*-condition. Unfortunately, they do not reveal competitive phases, nor do they provide error bars or uncertainties in phase boundaries. Such information, however, can be very helpful to rationalize experimental results. For instance, simultaneous appearance of $Ti_3N_4$ and $TiN_2$ in the same DAC experiment can be related to small differences in Gibbs energy between the two phases at 74 GPa and 2000 K [52,55,56]. Therefore, we provide relative Gibbs energy versus temperature data (ΔG-T) and relative Gibbs energy versus pressure data (ΔG-p) for Iron-Nitrogen phases. Effectively, these are "slices" cut through the manifold of G(p,T) data of all structures at constant p or at constant T, respectively. ΔG-T data at constant p may be particularly helpful for experimentalists, since in many experiments pressure is first set to a desired level, and only thereafter is Laser-heating applied to increase temperature.

In Fig. 3 (right) we present ΔG-T of Fe–N compounds at 58.5 GPa. Each line represents the Gibbs energy relative to $FeN_2$ for a system comprised of a structure with given composition plus appropriate amounts of nitrogen. The sequence of structures computed at 58.5 GPa then is $FeN_8 \overset{1200K}{\rightarrow} FeN_6 \overset{1340K}{\rightarrow} FeN_4 \overset{2000K}{\rightarrow} FeN_2 \overset{3120K}{\rightarrow} FeN \overset{3710K}{\rightarrow} Fe_4N_3 \overset{3935K}{\rightarrow} Fe_7N_3$, with the temperature of transition indicated above the arrow. Hence, computed data suggested that $FeN_2$ structure will be favorable between 2000 and 3120 K. The maximum driving force ΔG to attain the structure is at 2380 K, when it is favored by about 0.6 eV/$FeN_2$ over its closest competitor FeN. Likewise, Fig. 3 (left) shows ΔG-p of Fe–N compounds at 2380 K. We find the sequence of. $\gamma' - Fe_4N \overset{1.5\,GPa}{\rightarrow} Fe_7N_3 \overset{10.5\,GPa}{\rightarrow} Fe_3N_2\text{–II} \overset{15.5\,GPa}{\rightarrow} FeN \overset{27\,GPa}{\rightarrow} FeN_2 \overset{85\,GPa}{\rightarrow} FeN_4$ The thermodynamic stability of $FeN_2$ at 2380 K ranges from 26 to 85 GPa, with maximum ΔG of about 0.6 eV/$FeN_2$ relative to its competitor $FeN_4$

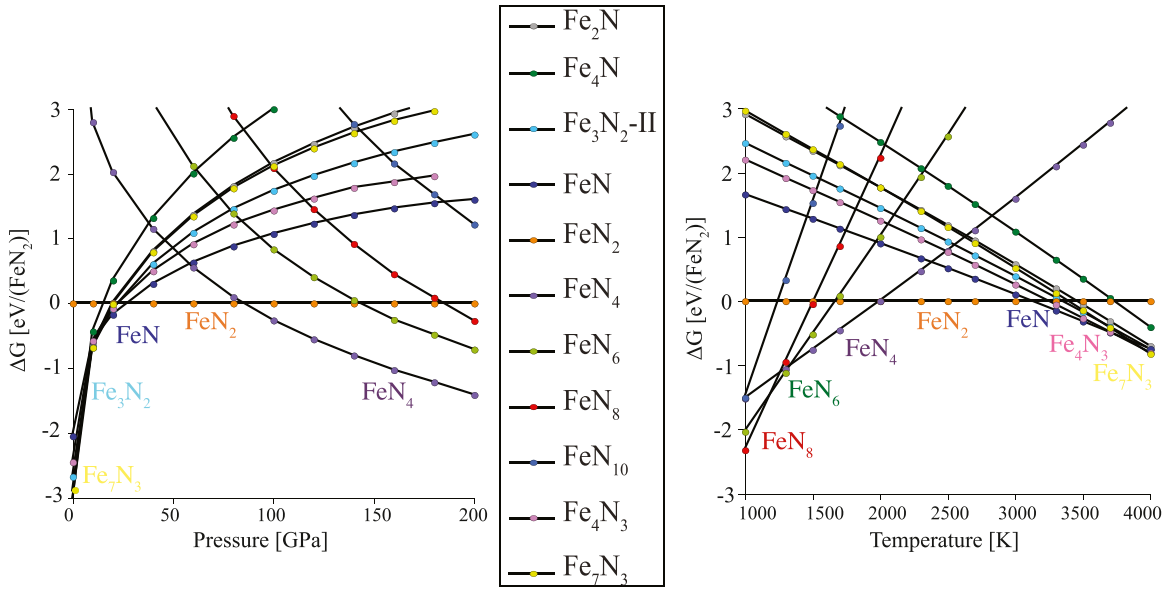


**Fig. 3.** (Left side of legend) Relative Gibbs energy versus pressure, Δ*G*-*p*, of Fe-N phases in excess nitrogen at 2380 K. (Right side of legend) Relative Gibbs energy versus temperature, Δ*G*-*T*, of Fe-N phases in excess nitrogen at 58.5 GPa. Symbols in the respective diagrams refer to structures listed in the boxed legend. Note that in each diagram energy refers to an overall composition $FeN_2$.

found at 58 GPa. We note that such data can be used to identify optimum *p,T*–conditions to synthesize a compound. And indeed, $FeN_2$ was synthesized using laser heated diamond anvil cell at pressure of 58.5 GPa and temperature between 2100 ± 200 K [7] – auspiciously close to the computed optimum conditions. A similar analysis (not shown here) yields a maximum driving force at 2340 K and 135 GPa to synthesize $FeN_4$ –– for which experimental conditions of 135 GPa and temperatures above 2000 K have been reported [7].

Favorable reaction kinetics will be required to synthesize $FeN_8$ with its structure displaying infinite chains of nitrogen. Fig. 1 indicates that the structure will become favorable only below 2000 K and that pressures exceeding 100 GPa are needed. It will be a challenge to attain this structure.

## 4. Summary and conclusion

We provide a comprehensive computation of the pressure-temperature phase diagram of the iron–nitrogen system for pressures up to 200 GPa and temperatures up to 4000 K. The work relies on a combination of Density Functional Theory computations with thermodynamic calculations that includes an assessment of the chemical potential of nitrogen at high pressure and high temperature. We identify stability fields of Fe-N structures in the presence of excess nitrogen under conditions of typical DAC experiments. We made "slices" of the phase diagram at constant pressure or at constant temperature to determine maximum driving force in order to validate our approach with experimental data. Based on a comparison of experimental and computational data, we estimate an uncertainty of our method of ± 300 K and ± 5 GPa. This assessment assumes, however, that experimental conditions are indeed corresponding to uniform presence of excess nitrogen and that observed structures are free of defects. When such conditions are not established, this may result in phases not identified here as "thermodynamically stable" – further enriching the landscape of feasible compounds.

## CRediT authorship contribution statement

**Hanof Alkhaldi:** Calculations, Formal analysis, Writing – original draft. **Peter Kroll:** Conceptualization, Methodology, Writing – review & editing.

## Declaration of Competing Interest

The authors declare that they have no known competing financial interests or personal relationships that could have appeared to influence the work reported in this paper.

## Acknowledgement

This work was supported by the National Science Foundation (NSF) through Award OISE-1743701. The work used the Extreme Science and Engineering Discovery Environment (XSEDE), which is supported by National Science Foundation Grant no. ACI-1548562. Additional computational work was made possible through generous grants by the Texas Advance Computing Center in Austin, TACC, Texas, and by the High Performance Computing facilities at UTA. H.A. acknowledges support by the Saudi Arabian Cultural Mission.

## References

[1] A. Zerr, G. Miehe, G. Serghiou, M. Schwarz, E. Kroke, R. Riedel, H. Fuess, P. Kroll, R. Boehler, Synthesis of cubic silicon nitride, Nature 400 (1999) 340–342.
[2] K. Landskron, H. Huppertz, J. Senker, W. Schnick, High-pressure synthesis of g-$P_3N_5$ at 11 GPa and 1500 °C in a multianvil assembly: a binary phosphorus(v) nitride with a three-dimensional network structure from PN4 tetrahedra and tetragonal PN5 pyramids, Angew. Chem.-Int. Ed. 40 (2001) 2643–2645.
[3] A. Zerr, G. Miehe, R. Riedel, Synthesis of cubic zirconium and hafnium nitride having $Th_3P_4$ structure, Nat. Mater. 2 (2003) 185–189.
[4] M.I. Eremets, A.G. Gavriliuk, I.A. Trojan, D.A. Dzivenko, R. Boehler, Single-bonded cubic form of nitrogen, Nat. Mater. 3 (2004) 558–563.
[5] E. Gregoryanz, C. Sanloup, M. Somayazulu, J. Badro, G. Fiquet, H.K. Mao, R.J. Hemley, Synthesis and characterization of a binary noble metal nitride, Nat. Mater. 3 (2004) 294–297.
[6] A. Zerr, G. Miehe, J.W. Li, D.A. Dzivenko, V.K. Bulatov, H. Hofer, N. Bolfan-Casanova, M. Fialin, G. Brey, T. Watanabe, M. Yoshimura, High-pressure synthesis of tantalum nitride having orthorhombic $U_2S_3$ type structure, Adv. Funct. Mater. 19 (2009) 2282–2288.
[7] M. Bykov, E. Bykova, G. Aprilis, K. Glazyrin, E. Koemets, I. Chuvashova, I. Kupenko, C. McCammon, M. Mezouar, V. Prakapenka, H.P. Liermann, F. Tasnadi, A.V. Ponomareva, I.A. Abrikosov, N. Dubrovinskaia, L. Dubrovinsky, Fe-N system at high pressure reveals a compound featuring polymeric nitrogen chains, Nat. Commun. 9 (2018) 2756.
[8] M. Bykov, E. Bykova, E. Koemets, T. Fedotenko, G. Aprilis, K. Glazyrin, H.P. Liermann, A.V. Ponomareva, J. Tidholm, F. Tasnadi, I.A. Abrikosov, N. Dubrovinskaia, L. Dubrovinsky, High-pressure synthesis of a nitrogen-rich inclusion compound $ReN_8$.x $N_2$ with conjugated polymeric nitrogen chains, Angew. Chem.-Int. Ed. 57 (2018) 9048–9053.

[9] D. Laniel, G. Weck, P. Loubeyre, Direct reaction of nitrogen and lithium up to 75 GPa: synthesis of the $Li_3N$, LiN, $LiN_2$, and $LiN_5$ compounds, Inorg. Chem. 57 (2018) 10685–10693.

[10] A. Zerr, R. Riedel, T. Sekine, J.E. Lowther, W.Y. Ching, I. Tanaka, Recent advances in new hard high-pressure nitrides, Adv. Mater. 18 (2006) 2933–2948.

[11] E. Horvath-Bordon, R. Riedel, A. Zerr, P.F. McMillan, G. Auffermann, Y. Prots, W. Bronger, R. Kniep, P. Kroll, High-pressure chemistry of nitride-based materials, Chem. Soc. Rev. 35 (2006) 987–1014.

[12] A. Salamat, A.L. Hector, P. Kroll, P.F. McMillan, Nitrogen-rich transition metal nitrides, Coord. Chem. Rev. 257 (2013) 2063–2072.

[13] C. Mailhiot, L.H. Yang, A.K. Mcmahan, Polymeric nitrogen, Phys. Rev. B 46 (1992) 14419–14435.

[14] P. Kroll, Hafnium nitride with thorium phosphide structure: physical properties and an assessment of the Hf-N, Zr-N, and Ti-N phase diagrams at high pressures and temperatures, Phys. Rev. Lett. 90 (2003) 125501.

[15] A.Y. Liu, M.L. Cohen, Structural properties and electronic structure of low-compressibility materials: b-$Si_3N_4$ and hypothetical b-$C_3N_4$, Phys. Rev. B 41 (1990) 10727–10734.

[16] J.C. Crowhurst, A.F. Goncharov, B. Sadigh, C.L. Evans, P.G. Morrall, J.L. Ferreira, A.J. Nelson, Synthesis and characterization of the nitrides of platinum and iridium, Science 311 (2006) 1275–1278.

[17] S.T. Oyama, The Chemistry of Transition Metal Carbides and Nitrides, Blackie Academic & Professional; Chapman & Hall, Glasgow, Scotland, 1996.

[18] J.F. Adler, Q. Williams, A high-pressure X-ray diffraction study of iron nitrides: implications for Earth's core, J. Geophys. Res.-Solid Earth 110 (2005) B01203.

[19] M. Roskosz, M.A. Bouhifd, A.P. Jephcoat, B. Marty, B.O. Mysen, Nitrogen solubility in molten metal and silicate at high pressure and temperature, Geochim. Cosmochim. Acta 121 (2013) 15–28.

[20] K.D. Litasov, A.F. Shatskiy, Composition of the Earth's core: a review, Russ. Geol. Geophys 57 (2016) 22–46.

[21] K.D. Litasov, A. Shatskiy, D.S. Ponomarev, P.N. Gavryushkin, Equations of state of iron nitrides e-$Fe_3N_x$ and g-$Fe_4N_y$ to 30 GPa and 1200 K and implication for nitrogen in the Earth's core, J. Geophys. Res.-Solid Earth 122 (2017) 3574–3584.

[22] Y.K. Zhuang, X.W. Su, N.P. Salke, Z.X. Cui, Q.Y. Hu, D.Z. Zhang, J. Liu, The effect of nitrogen on the compressibility and conductivity of iron at high pressure, Geosci. Front. 12 (2021) 983–989.

[23] H. Jacobs, D. Rechenbach, U. Zachwieja, Structure determination of g′-$Fe_4N$ and e-$Fe_3N$, J. Alloy. Compd. 227 (1995) 10–17.

[24] K. Guo, D. Rau, J. von Appen, Y. Prots, W. Schnelle, R. Dronskowski, R. Niewa, U. Schwarz, High pressure high-temperature behavior and magnetic properties of $Fe_4N$: experiment and theory, High. Press. Res. 33 (2013) 684–696.

[25] H.A. Wriedt, N.A. Gokcen, R.H. Nafziger, The Fe-N (iron-nitrogen) system, Bull. Alloy Phase Diagr. 8 (1987) 355–377.

[26] W.P. Clark, S. Steinberg, R. Dronskowski, C. McCammon, I. Kupenko, M. Bykov, L. Dubrovinsky, L.G. Akselrud, U. Schwarz, R. Niewa, High-pressure NiAs-type modification of FeN, Angew. Chem.-Int. Ed. 56 (2017) 7302–7306.

[27] K. Niwa, T. Terabe, D. Kato, S. Takayama, M. Kato, K. Soda, M. Hasegawa, Highly coordinated iron and cobalt nitrides synthesized at high pressures and high temperatures, Inorg. Chem. 56 (2017) 6410–6418.

[28] D. Laniel, A. Dewaele, G. Garbarino, High pressure and high temperature synthesis of the iron pernitride $FeN_2$, Inorg. Chem. 57 (2018) 6245–6251.

[29] M. Bykov, S. Khandarkhaeva, T. Fedotenko, P. Sedmak, N. Dubrovinskaia, L. Dubrovinsky, Synthesis of $FeN_4$ at 180 GPa and its crystal structure from a submicron-sized grain, Acta Crystallogr. Sect. E-Crystallogr. Commun. 74 (2018) 1392–1395.

[30] M. Hasegawa, T. Yagi, Systematic study of formation and crystal structure of 3d-transition metal nitrides synthesized in a supercritical nitrogen fluid under 10 GPa and 1800 K using diamond anvil cell and YAG laser heating, J. Alloy. Compd. 403 (2005) 131–142.

[31] C.M. Fang, M.A. van Huis, H.W. Zandbergen, Stability and structures of the e-phases of iron nitrides and iron carbides from first principles, Scr. Mater. 64 (2011) 296–299.

[32] Z.Y. Wang, Y.C. Li, H.T. Li, I. Harran, M.Z. Jia, H. Wang, Y.Z. Chen, H.Y. Wang, N.N. Wu, Prediction and characterization of the marcasite phase of iron pernitride under high pressure, J. Alloy. Compd. 702 (2017) 132–137.

[33] Y.Z. Chen, X.Y. Cai, H.Y. Wang, H.B. Wang, H. Wang, Novel triadius-like $N_4$ specie of iron nitride compounds under high pressure, Sci. Rep. 8 (2018) 10670.

[34] F.B. Jiao, C.Y. Zhang, W.Y. Xie, High-pressure FeNx: stability, phase transition, and energetic characteristic, J. Phys. Chem. C 124 (2020) 19953–19961.

[35] N.E. Sagatov, D.N. Sagatova, P.N. Gavryushkin, K.D. Litasov, Fe–N system at high pressures and its relevance to the earth's core composition, Cryst. Growth Des. 21 (2021) 6101–6109.

[36] N. Sagatov, P.N. Gavryushkin, T.M. Inerbaev, K.D. Litasov, New high-pressure phases of $Fe_7N_3$ and $Fe_7C_3$ stable at Earth's core conditions: evidences for carbon-nitrogen isomorphism in Fe-compounds, Rsc Adv. 9 (2019) 3577–3581.

[37] L.L. Wu, R.F. Tian, B. Wan, H.Y. Liu, N. Gong, P. Chen, T.D. Shen, Y.S. Yao, H.Y. Gou, F.M. Gao, Prediction of stable iron nitrides at ambient and high pressures with progressive formation of new polynitrogen species, Chem. Mater. 30 (2018) 8476–8485.

[38] A. Kartsev, O.D. Feya, N. Bondarenko, A.G. Kvashnin, Stability and magnetism of FeN high-pressure phases, Phys. Chem. Chem. Phys. 21 (2019) 5262–5273.

[39] D. Laniel, A. Dewaele, S. Anzellini, N. Guignot, Study of the iron nitride FeN into the megabar regime, J. Alloy. Compd. 733 (2018) 53–58.

[40] P. Hohenberg, W. Kohn, Inhomogeneous electron gas, Phys. Rev. B 136 (1964) B864–B871.

[41] G. Kresse, Ab-initio molecular-dynamics for liquid-metals, J. Non-Cryst. Solids 193 (1995) 222–229.

[42] G. Kresse, J. Hafner, Ab-initio molecular-dynamics simulation of the liquid-metal amorphous-semiconductor transition in germanium, Phys. Rev. B 49 (1994) 14251–14269.

[43] G. Kresse, J. Furthmuller, Efficiency of ab-initio total energy calculations for metals and semiconductors using a plane-wave basis set, Comp. Mater. Sci. 6 (1996) 15–50.

[44] P.E. Blöchl, Projector augmented-wave method, Phys. Rev. B 50 (1994) 17953–17979.

[45] G. Kresse, D. Joubert, From ultrasoft pseudopotentials to the projector augmented-wave method, Phys. Rev. B 59 (1999) 1758–1775.

[46] J.W. Sun, A. Ruzsinszky, J.P. Perdew, Strongly constrained and appropriately normed semilocal density functional, Phys. Rev. Lett. 115 (2015) 036402.

[47] M.H. Wetzel, M.R. Schwarz, A. Leineweber, High-pressure high-temperature study of the pressure induced decomposition of the iron nitride g′-$Fe_4N$, J. Alloy. Compd. 801 (2019) 438–448.

[48] A.R. Oganov, Y.M. Ma, A.O. Lyakhov, M. Valle, C. Gatti, Evolutionary crystal structure prediction as a method for the discovery of minerals and materials, in: R. Wentzcovitch, L. Stixrude (Eds.), Theoretical and Computational Methods in Mineral Physics: Geophysical Applications, 2010, pp. 271–98.

[49] J. Zhang, A.R. Oganov, X.F. Li, H.Y. Niu, Pressure-stabilized hafnium nitrides and their properties, Phys. Rev. B 95 (2017) 020103.

[50] P. Kroll, Pathways to metastable nitride structures, J. Solid State Chem. 176 (2003) 530–537.

[51] P. Kroll, T. Schröter, M. Peters, Prediction of novel phases of tantalum(V) nitride and tungsten(VI) nitride that can be synthesized under high pressure and high temperature, Angew. Chem.-Int. Ed. 44 (2005) 4249–4254.

[52] H. Alkhaldi, P. Kroll, Chemical potential of nitrogen at high pressure and high temperature: application to nitrogen and nitrogen-rich phase diagram calculations, J. Phys. Chem. C 123 (2019) 7054–7060.

[53] R.T. Jacobsen, R.B. Stewart, M. Jahangiri, Thermodynamic properties of nitrogen from the freezing line to 2000 K at pressures to 1000 MPa, J. Phys. Chem. Ref. Data 15 (1986) 735–909.

[54] H. Alkhaldi, P. Kroll, Computing the tantalum-nitrogen phase diagram at high pressure and high temperature, J. Phys. Chem. C 124 (2020) 22221–22227.

[55] V.S. Bhadram, D.Y. Kim, T.A. Strobel, High-pressure synthesis and characterization of incompressible titanium pernitride, Chem. Mater. 28 (2016) 1616–1620.

[56] V.S. Bhadram, H.Y. Liu, E.S. Xu, T.S. Li, V.B. Prakapenka, R. Hrubiak, S. Lany, T.A. Strobel, Semiconducting cubic titanium nitride in the $Th_3P_4$ structure, Phys. Rev. Mater. 2 (2018).

[57] $Fe_3N_2$ adopts space group symmetry *Fdd*2 (43) with lattice parameters a = 6.94, b = 6.08, and c = 6.76. Atoms are Fe at (0, 0, -0.2239), N1 at (-0.1674, 0.0624, 0.2292), and N2 (0.3048, 0.0299, 0.4493), in.

[58] Y.L. Li, S.N. Wang, A.R. Oganov, H.Y. Gou, J.S. Smith, T.A. Strobel, Investigation of exotic stable calcium carbides using theory and experiment, Nat. Commun. 6 (2015) 6974.

[59] $FeN_8$ adopts space group symmetry *P*-1 (1) with lattice parameters a = 4.14, b = 4.31, c = 3.44; and a = 110.7°, b = 83.43°, g = 72.25°. Atoms are Fe at (0, 0,0.5), N1 at (-0.13171, -0.23095, -0.22887), N2 at (-0.03462, 0.36362, -0.00334), N3 at (-0.44232, 0.12528, 0.48929), and N4 at (0.40971, 0.29414, 0.27986), in.

[60] $FeN_8$-$N_2$ adopts space group symmetry *Immm* (71) with lattice parameters a = 3.64, b = 6.38, and c = 5.87. Atoms are Fe at (0, 0, 0), N1 at (0.18074, -0.32342, 0.3121), and N2 at (-0.33998, 0.5, 0) (data at 102 GPa), in.

[61] M. Bykov, S. Chariton, E. Bykova, S. Khandarkhaeva, T. Fedotenko, A.V. Ponomareva, J. Tidholm, F. Tasnadi, I.A. Abrikosov, P. Sedmak, V. Prakapenka, M. Hanfland, H.P. Liermann, M. Mahmood, A.F. Goncharov, N. Dubrovinskaia, L. Dubrovinsky, High-pressure synthesis of metal-inorganic frameworks $Hf_4N_{20}{\cdot}N_2$, $WN_8{\cdot}N_2$, and $O_{s5}N_{28}{\cdot}3N_2$ with polymeric nitrogen linkers, Angew. Chem.-Int. Ed. (2020) 7.